Understanding Gold Alloy Features From Thermodynamic Phenomena

AUTHORS

Dr. Patrizio Sbornicchia, Stefano Rappo, Damiano Zito, Valerio Doppio, Federica Tiso, Gisela Cepeda
Progold S.p.A.
Trissino (VI), Italy

1. INTRODUCTION

The colored gold alloys are generally a ternary matrix of three elements such as gold, copper and silver. Their association is so favorable and stable that most natural precious nuggets found around the world reflect this general composition. The variable content of copper and silver not only dictates the color but also a great part of the metallurgical behavior of the gold alloy, even if the presence of other additives is commonly required to improve the opto-mechanical characteristics to the level demanded by the modern market.

Lost-wax investment casting is a very ancient and reliable production process to obtain accurate items, and it is typically performed by pouring molten alloys into refractory molds.[1] In ideal conditions, the liquid alloy fills the cavities of the mold without interactions or turbulence and, consequently, the resulting surface quality of the solid items is very smooth and the integrity of the parts is maintained down to the finest details. The features of form-filling and inner porosity constitute the castability performance of the alloy. Roughness is also included in this definition but, being a surface characteristic of the solid, it is less important, especially because it can be easily removed by the usual finishing techniques. This is particularly true for low roughness, the magnitude of which does not affect the detail resolution of the cast. Unfortunately, real castings are often affected by several volume defects that may lead to rejects. The family of volume defects is highly populated, but the main flaws are porosity and incomplete filling of parts. Other defects such as larger hard-spot clusters can menace the final quality of the items, but they are usually negligible if present as small isolated particles with a size less than five micrometers.

The porosity in a casting mainly arises from metal shrinkage during solidification, gas released during eventual thermal decomposition of the investment mold, and oxygen or other gas exsolving from the melt during solidification. On the other hand, mold-filling is affected by the melting range of the alloys, their thermal conductivity, viscosity and surface tension, the wettability of the mold surface and the gas permeability of the mold. There can even be cross-interactions between thermal shrinkage and form-filling causes. In order to best address shrinkage phenomena, it may be more convenient to consider the dynamics related to the entire solidification process as a whole. Thus it may be possible to develop a deeper understanding of which detailed processes occurring during these extremely complex transformation stages matter the most in achieving better castings.

Since solidification includes a physical transition from liquid to solid phase, it is therefore good to start by taking into consideration the nature of the liquid phase. In general, today, there is not an exhaustive knowledge of the structure of the liquid state, but some generalizations can be made. The liquid state can be thought of as an intermediate state of matter between the gaseous state, in which widely-spaced and mobile atoms are free to occupy fully random positions with respect to each other, and the crystalline solid state, in which atoms occupy specific positions and spacing according to precise lattice rules. Direct investigations have shown that the substantial difference between a solid metal and its liquid is constituted by different degrees of order in their atomic distribution. It can be demonstrated that the liquid phase is characterized by short range order, where each atom is loosely, symmetrically and roughly equidistantly surrounded by its nearest neighbor atoms, creating a sort of local prearrangement without additional longer-range coordination and order.

In the case of solid metal, such neighbor-to-neighbor coordination is extended symmetrically and indefinitely towards each direction of the space occupied by the crystal, defining a long-range order. Important properties of the solid and the liquid states are influenced by the different degrees of order of their constituent atoms. For example, a temperature increase in either solid or liquid metals implies an increase of the amplitude and frequency of the atomic vibrations, which therefore tend to occupy wider spacings, leading to a density reduction of the material. Accordingly, atomic diffusion increases in both states in large part because the warmer structures are “looser.”

A very important feature for alloy casting turns out to be the fluidity or castability, generally measured by the percentage of penetration of the liquid metal in a standard test mold, as we will see later. This mold-filling property has a very complex nature, due to the large number of variables which can influence its magnitude. In general, it depends directly on the temperature and inversely on the viscosity, the surface tension, but also on the addition of alloying elements or the presence of heterogeneities such as oxide films, gas, intermetallic compounds and other refractory particles. Fluidity is higher in pure metals or eutectic alloys. The increase of the structural order during the transition from liquid into solid provokes in each alloy an abrupt variation of almost all its properties, even those which do not depend on the crystalline structure. Indeed, a number of material properties depend on the microstructural aggregation of single crystals (grains), which, in turn, are connected to the solidification process. The specific volume (1/density) is another important property that suddenly varies during phase transition between the solid and liquid states. In common situations, a reduction of the volume is encountered by passing from the liquid phase into the solid one, but there are exceptions to this behavior, for instance, with gallium, silicon, germanium and a few other elements.[2]

With pure metals, such as gold, this volume decrease can be split into three parts. The first one is gradual during the liquid cooling, the second is abrupt arising from the liquid-to-solid transition and the last one, again, gradual from solid mass shrinkage. The second part, regarding solidification shrinkage from liquid to the solid phase is of utmost importance because in it there is a change from a short-range order to a long-range one, where the attractive forces are stronger than those existing in the same liquid metal so that during solidification, the interatomic distances generally decrease significantly.

Metals and alloys definitively undergo dimensional changes in response to variations in temperature, a phenomenon that has critical implications for industries that process these materials at high temperatures. Specific practices, such as investment casting and injection molding versus hot solid working processes like forging, rolling and drawing, can be significantly influenced by thermal stresses and strains that arise from temperature variations. These lead to poor-quality products without an adequate control process. Improper process parameters and alloy compositions can generate incomplete parts, microporosity, residual stresses and distortions that can lead to the formation of cracks and failures. Hence, the optimization of such processes calls for the use of sophisticated computer models that require comprehensive data on the thermal expansion characteristics of the material. The availability of data for the thermal expansion coefficient (CTE) at elevated temperatures then becomes a key issue.[3]

The main purpose of this research is to find a possible correlation between thermodynamic quantities and technological properties of gold alloys in order to provide a practical tool for estimating, at least on a qualitative basis, the metallurgical behavior of the alloys by only considering their starting composition. This useful predictive tool could result in a remarkable reduction in the choice and characterization of the precious alloys, reducing or avoiding long and expensive casting and mechanical tests. Among the several properties that affect the technological behavior of gold alloys we can take into account are melting range, solid-state transformations, density variation during solidification and cooling, hardening additives and grain size.

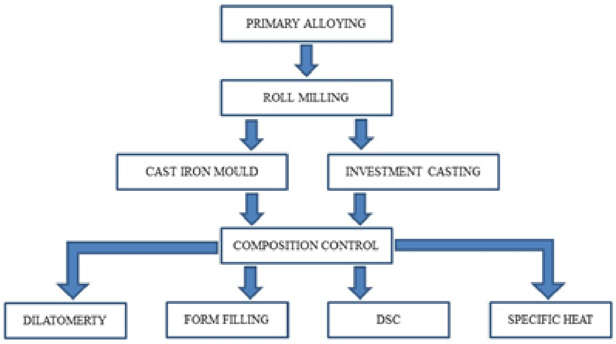

Figure 1 Research structure flowchart

EXPERIMENTAL METHODS

The gold alloys that were used in this research were produced using high purity elements (99.99 wt.%) and prepared using a double casting in order to ensure a better homogenization of the raw materials, whose purity was controlled through Inductively Coupled Plasma Optical Emission Spectroscopy (ICP-OES) and Wavelength Dispersive X-Ray Fluorescence (WDXRF). The preparation of the alloys consisted of a first casting in an argon-protected system, followed by rolling of the cast ingot to ensure a further homogenization in the solid state and followed by a second casting either in a cast iron mold to obtain a pair of dilatometry samples or in traditional flasks for the form-filling tests. In both cases, casting was always done in a protected environment (Figure 1).

The preparation of the dilatometry specimens (Netzsch DIL 402 Supreme Expedis®) and the differential scanning calorimetry specimens (Netzsch DSC Jupiter® STA 449,) was done by melting primary granules in argon-protected crucibles and casting the alloy into an iron ingot mold that was specially prepared for the simultaneous formation of two precious metal cylinders (Figure 2). These cylinders, machined and polished, were tested as a pair of analytic specimens for dilatometry in order to have an idea

Figure 2 As-cast dilatometry specimens and polished cylinders ready for measurement

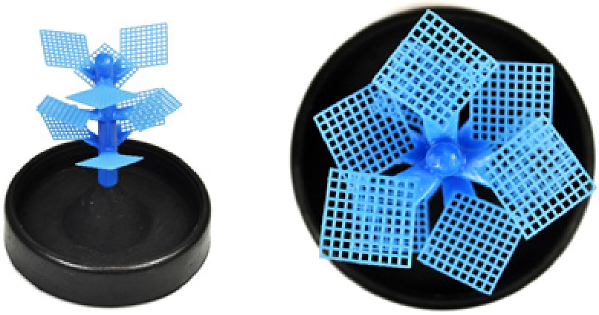

Figure 3 Structure of the wax tree for form filling test

of the technique's reproducibility and to give a more reliable averaged value. The total volume of the internal shape of the iron ingot mold is about 10 cm^3, which allows a proper riser capable of absorbing the shrinkage of the metallic mass and avoiding porosities. The dilatometric specimens were cylinders with a diameter of 6.34 ±0.10 mm and a height of 12.00 ±0.50 mm. Both ends of each cylinder must be as coplanar as possible, with a maximum admissible run-out of 0.10 mm.

Dilatometry measurements were executed in an argon chamber (99.999%) and the alloys were further protected by the insertion of an oxygen trap system (OTS®). The presence of residual oxygen can be critical because oxidation of the sample would lead to spurious results and false interpretations. The OTS system allows for effective reduction of the oxygen partial pressure in the vicinity of the sample by means of a ceramic support. The residual oxygen content remaining after evacuation is thereby almost entirely eliminated (residual O_2 vol.% < 1ppm). The metal test cylinders were placed in isostatically molded graphite capsules equipped with moving pistons, which allowed the alloy volume to vary but prevented leaking molten metal into the alumina heating holder. The measurement range used in this research was from room temperature up to 1200°C (2192°F). The temperature scan was 10°C/min up to 600°C (18°F/min up to 1112°F) and then decreased to 5°C/min (9°F/min) to higher temperature. Thus, the dilatometer was used to evaluate the thermal expansion coefficient (CTE) of metals and alloys in the solid, liquid and two-phase states.

The expansion of any material with temperature can be quantified in terms of increasing linear dimension, such as the length of a specimen. The simplest form for coefficient of linear thermal expansion of any material can be given as the fractional increase in length per unit rise in temperature. Its physical unit in the international system is K^{-1}, but in the technological field its equivalent is given as µm/mK and typical values for metals and alloys are in the range $10–30\cdot10^{-6}$ K^{-1}. It is generally found that materials with higher melting temperatures have lower thermal expansion coefficients. It is important to note that the coefficient of thermal expansion (CTE) is a temperature-dependent property that can somewhat change into a temperature range and thus can be stated as a single averaged value (CTE_a). In this research we measured the average coefficient of linear expansion for a solid from room to solidus temperature ($CTE_{a(sol)}$) and from liquidus temperature to 1200°C ($CTE_{a(liq)}$). However, in some instances the occurrence of phase transitions will cause discontinuities in the value of the coefficient.[3]

During heating and melting, the increase of material volume pushes the piston toward the instrument-sensing pushrod, and this relative motion is recorded and elaborated for deriving thermal expansion coefficient. The precision of the volume expansion or density change across the melting range and beyond into the liquidus temperature required carefully taking into account the container expansion by means of preliminary calibrations without specimens.

The measurement error of the density at the liquidus temperature was usually less than 1% with respect to literature values.[4] Similarly, the disparity between the measurements of two specimens of the same material at the liquid state shows a difference less than 1%. The absolute variation of density

across the melting range ($\Delta d_{sol-liq}$) is the one parameter that may most affect form-filling and the formation of porosity inside cast items.
The form-filling tests of the precious alloys were performed with identical wax patterns having a square network structure.[5,6] These patterns were obtained by wax injection into the same rubber mold and have a square unit cell of 1.80 x 1.80 mm with a thickness of 0.80 mm (Figure 3). The compositional conformity and uniformity were carried out on the top and bottom ingate (feed sprue) of the cast trees. Three different levels of patterns were used with a distance of 23 mm vertically between them. Also, each level contains three items disposed in a trigonal symmetry to favor filling with a grade of 15° towards the top of the structure (Figure 3). This configuration was chosen based on literature[7] and past experience with this shape, demonstrating a high degree of consistency.

The melting tests were carried out in a programmed machine, thus limiting the number of parameters that, through casual fluctuations or measurement uncertainties, could have affected the resulting cast pieces in a non-controllable way. For example, only gravity was mostly employed during casting. No pressure was applied after emptying the crucible in order to avoid the effect an imprecise pressurizing delay can have on the filling and solidification of the patterns. Furthermore, an increase in pressure might cause cracks in the investment mold that are consequently filled with metal, adding fins to the pattern geometry.

One of the most interesting tests was the study of the relation between the characteristic melting temperature range of an alloy and the degree of form-filling in the investment mold. These tests yielded a correlation between form-filling and the concentrations of the elements that modify the melting range density change. Additional parameters of the alloy such as its viscosity and contact angle to the investment at the liquid state could be a future research topic in order to improve our understanding of form-filling.

The thermal analyses were performed by following the standard method (ASTM E793) with scanning rate of the temperature set at 5°C/min and specimen mass of about 20 mg in an argon-protected atmosphere and adoption of a trap system (OTS®). The specific heat measurement was performed with a scanning rate of 20°C/min in the same protection conditions and heavier mass (85 mg) in order to increase the sensitivity of analysis. The ratio method was used for calculation of specific heat by using a pure sapphire disk (85 mg) as reference material. In any case, all experimental measurements (DIL, DSC, CTE) used as-cast materials, and the corresponding trials with annealed specimens may give slightly different results.

RESULTS AND DISCUSSION

Dilatometry

Dilatometry is a very relevant technique that is able to give qualitative and quantitative information on size changes of material as a function of temperature. The typical parameters used in this technological field are linear and volumetric thermal expansion coefficient and density variation both in the solid and liquid states. These features are very important in jewelry manufacturing to estimate possible mechanical stress, shrinkage porosity during solidification and size estimate modifications under cooling. The measurements were focused on the determination of average linear coefficient of thermal expansion (CTE_a) in the solid state, the relative volumetric change ($\Delta V/V_0$) during solidification and the density variation in the molten phase.

Variations of volume and density at high temperature in an alloy going from the molten to the solid state are evident in terms of the shrinkage that any pure metal or gold alloy exhibits. This phenomenon can also affect the castability and, consequently, the degree of filling of the investment mold pattern, while dimensional changes in the solid state during cooling can place large strains on assembled jewelry and create ruptures in the weakest areas. On the other hand, dimensional variations taking place in the melting range can influence the degree of filling of an alloy. Indeed, if the material tends to contract a lot during solidification due to crystallization, then it also tends to create denser grains. This means that the grains are less voluminous than the surrounding liquid and consequently favor the filling of the patterns. For example, a simple stone-set ring can be better filled from molten alloys if the crystallizing nuclei are denser with respect to the parent liquid because the thinner channels tend to remain open to the melt flow (Figure 4). This phenomenon is quite different from what happens in the presence of grain refiners. From the results obtained, grain refiners seem to only render the crystalline nuclei smaller and more abundant and not significantly denser, so form-filling could not be increased in a relevant way. Moreover, the higher number of smaller nuclei could increase the solidification speed of the molten mass so form-filling may remain similar to casting an alloy without grain refiners and thus bigger crystallizing grains, with the only possible advantage of improving the resolution of casting for finest details of the already filled parts.

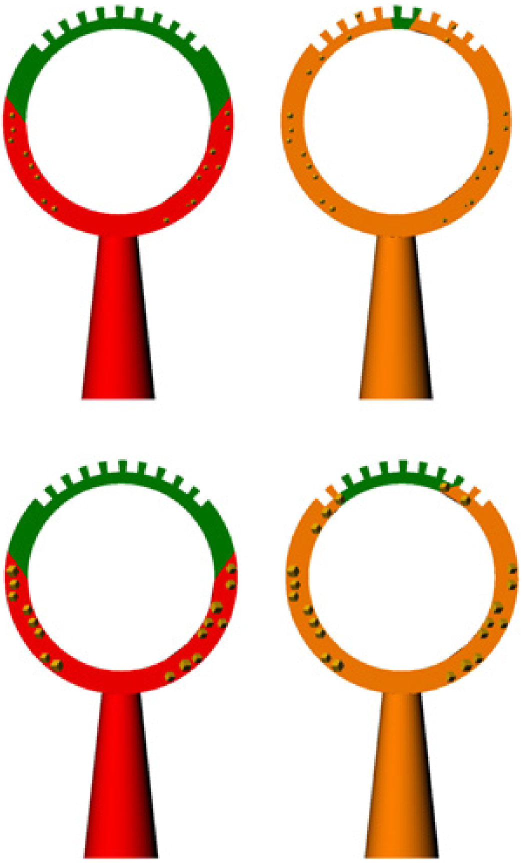

Figure 4 Higher filling due to formation of denser (top) and less dense grains (bottom)

On the other hand, if an alloy tends to expand and diminish its density during solidification, crystalline nuclei more voluminous than the surrounding liquid will form and hinder the flux of metallic mass to the patterns (Figure 4). However, dimensional shrinkage of an alloy can be modified by different factors such as the addition of additives, by the ingate structure and casting parameters.

In general, metallic elements that possess a compact atomic structure at the solid state tend to lose crystalline regularity during melting because of the thermal agitation that increases the average distance between the atoms, and this decreases the density at the liquid state. On the other hand, metalloid elements used in jewelry such as silicon, germanium and metals such as gallium[8] develop a more open structure during solidification due to the nature of their covalent bonds among the atoms, which have preferential directions. Usually, these elements not only show a higher density at the liquid state (d_{liq}) than in the solid state (d_{sol}), but they also behave in a more metallic way in their liquid conditions (Table 1).

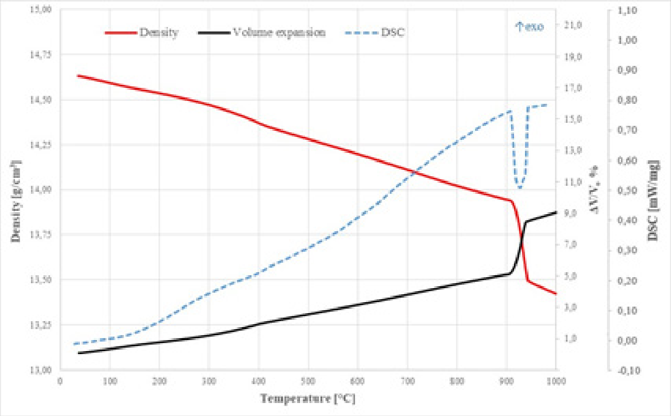

Figure 5 Typical dilatometry integrated with differential scanning calorimetry for 18K nickel white-gold alloy

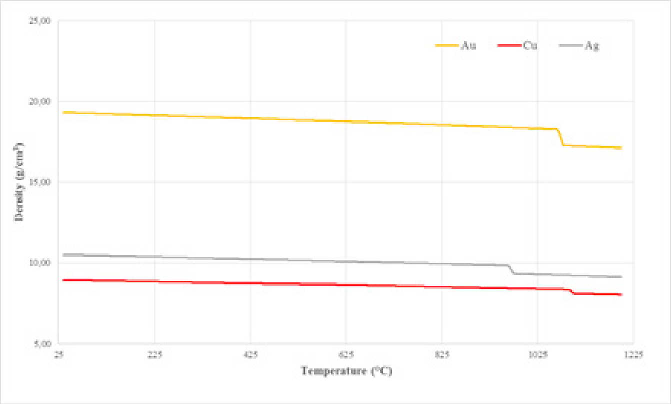

Figure 6 Density of pure gold, silver and copper as a function of temperature

Table 1 Room density of jewelry elements and at melting point with coefficient of linear thermal expansion[9,10,11]

Element	**d_{RT} [g·cm^{-3}]**	**dm_{LIQ} [g·cm^{-3}]**	**CTE$_a$ [10^{-6} K^{-1}]**
Au	19.30	17.31	14.2
Ag	10.49	9.30	19.0
Cu	8.93	7.94	16.5
Pd	12.02	10.38	11.8
Ni	8.90	7.81	13.3
Si	2.33	2.57	2.6
Ge	5.32	5.60	6.0
Ga	5.91	6.09	21.5

A typical dilatometric analysis can give direct access to meaningful data such as the average linear expansion coefficient (CTE$_a$), the percent volume change ($\Delta V/V_{0(\%)}$) and density variation as a function of the physical state and even during phase transitions, as illustrated for a classical 18K nickel white-gold alloy (Figure 5). As a general trend, gold alloys show a very linear density variation after 400°C (752°F) up to solidus temperature, together with a corresponding linear volume change. The initial linear behavior is interrupted by a sudden decreasing of density at the solidus temperature around 910°C (1670°F) and rapid increase of the alloy volume, which is the point at which melting begins.
Through the melting range, these parameters vary quite linearly up to liquidus temperature, where another abrupt change is encountered because the melting is complete. At the liquidus point the density has decreased about 7.7% from the room-temperature value, and the relative volume is increased about 8.4% compared to room-temperature conditions.

The liquid alloys above liquidus behave analogously to the solid phase with, again, milder rates of decreases in density and relative volume. At temperature below 400°C the density and relative volume curves can display deviations from the linearity because of order/disorder transition that can give a temporary significant density increase, especially for 18K red-gold alloys.
The three principal components that constitute most of the precious metal matrices used in jewelry are gold, silver and copper, each one of them presenting a distinctive volumetric behavior during heating and melting. Three other metals commonly used in commercial jewelry alloys, namely nickel (Ni), palladium (Pd) and zinc (Zn), were also included in this study.
Experiments began with dilatometry on the three pure principal component metals and the three pure common alloying metals in order to understand their baseline volumetric behaviors upon heating. The influence of small additions of silver (Ag), zinc and the metalloids germanium (Ge) and silicon (Si) were measured in an 18K Au-Cu matrix. Dilatometry was concluded by studying some alloys similar to those available in the marketplace.

The density of the principal metals Au, Ag and Cu as a function of temperature (Figure 6) shows a slow and steady decrease in the solid state before decreasing abruptly at the melting point. This is particularly valid for silver and gold (Table 2). In the case of pure liquid gold, the structure is well established. X-ray studies of the liquid phase show that gold may be classified with other typical metals as having a structure best described in terms of nearly close-packed assemblies of spherical atoms.8 According to this model, the liquid is essentially a disordered version of the crystal structure in the metallic solid, which is also close-packed face-center cubic (FCC). This disordering, or absence of long-range order, in the liquid gives rise to a change in density. When the densities of liquid and solid gold are compared at the freezing point, 1064°C (1947°F), the greater density of the solid, 18.3 g/cm3 compared with 17.3 g/cm^3 for liquid gold, shows that gold, like any typical metal, must shrink on freezing. For gold the percentage volume change on solidification is 5.1%.[8]

Table 2 Density percent change of some pure elements used in jewelry manufacturing [8]

ELEMENT	d_{RT} [g·cm^{-3}]	$\Delta d_{\%RT\text{-}sol}$ [g·cm^{-3}]	$\Delta d_{\%sol\text{-}liq}$ [g·cm^{-3}]	Δd%RT-liq [g·cm^{-3}]
Au	19.32	5.11	5.26	10.37
Ag	10.49	6.11	5.08	11.19
Cu	8.93	6.57	4.30	10.87
Ni	8.90	5.45	6.80	12.25
Zn	7.13	3.35	4.50	7.85
Pd	12.02	5.20	8.44	13.64

In other words, the experimentally measured density change across the solid temperature range ($\Delta d_{RT\text{-}sol}$ = 0.987 g/cm^3) is about the same as that measured at melting ($\Delta d_{sol\text{-}liq}$ = 1.015 g/cm^3), giving a total variation of ($\Delta d_{RT\text{-}liq}$ = 2.002 g/cm^3), which is equal to about 10% of the density at room temperature (Table 2). However, in the case of pure silver and copper, the total density change in the solid state is greater than at their melting points (Table 3), which is different from the case of pure gold.

Table 3 Density change at the melting point for some pure elements used in jewelry manufacturing [8]

ELEMENT	T_m [°C]	$r_{covalent}$ [pm]	d_{RT} [g·cm^{-3}]	$CTE_{a(sol\text{-}liq)}$ [10^{-6} K^{-1}]	d_{sol} [g·cm^{-3}]	d_{liq} [g·cm^{-3}]	$\Delta d_{RT\text{-}sol}$ [g·cm^{-3}]	$\Delta d_{sol\text{-}liq}$ [g·cm^{-3}]	$\Delta d_{RT\text{-}liq}$ [g·cm^{-3}]
Au	1064.4	136	19.32	17.25 – 64.73	18.313	17.298	0.987	1.015	2.002
Ag	961.9	145	10.49	23.16 – 94.15	9.849	9.316	0.641	0.533	1.174
Cu	1084.9	132	8.93	20.98 – 80.08	8.341	7.957	0.589	0.384	0.973
Ni	1453.0	124	8.90	13.30 – n.d.	8.415	7.810	0.485	0.605	1.090
Zn	420.0	122	7.13	39.70 – n.d.	6.891	6.570	0.239	0.321	0.560
Pd	1552.0	139	12.02	11.76 – n.d.	11.395	10.380	0.625	1.015	1.640

The density changes of nickel, zinc and palladium were determined by using indirect methods instead of being measured with the dilatometer in order to avoid eventual reactions between the current crucible (graphite) for Ni and Pd, and because of the rather high vapor pressure of zinc in the liquid state. The liquid density at the melting point is a value that can be found in literature[4] while the density of the alloy just before melting can be calculated using the average coefficient of thermal expansion. By using these parameters, it is possible to estimate the approximate density of the alloy at the moment just before melting.

The highest average coefficient of thermal expansion in the solid state (CTE_a) belongs to pure silver, which tends to expand more both in the solid state and in the liquid state, compared to Au and

Cu under the same conditions. Gold, meanwhile, provides the most dimensional stability given the same conditions.
Alloys constituted by these three elements (Au, Ag, Cu) already show a substantial reduction of density change (Tables 4, 5 and 6) with respect to pure gold. This phenomenon can be attributed, at least partly, to a mixing at the atomic level with copper, an element that shows considerably smaller density and relative volume variations at melting (Tables 2 and 3). Extensive solid solubility of Cu in Au alloys is due to a notable degree of interchangeability between these elements that derives from their similar atomic dimension and an identical crystallographic structure since all of them are face-centered cubic (FCC).

Table 4 Compositions for the determination of the partial derivatives of the single additives

Alloy	**Au [wt.%– at.%]**	**Cu [wt.%– at.%]**	**Ag [wt.%– at.%]**	**Zn [wt.%– at.%]**	**Ge [wt.%– at.%]**	**Si [wt.%– at.%]**
A	100.0–100.0					
B	75.00–49.18	25.00–50.82				
C	75.00–49.21	23.99–48.79		1.01–2.00		
D	75.00–49.33	23.89–48.68			1.12–2 .00	
E	75.00–49.05	24.89–50.45				0.109–0.500
F	75.00–49.87	23.35 – 48.13	1.65–2.00			
G	75.00–49.35	22.87–46.65		1.01–2.00	1.12–2.00	
H	75.00–49.21	22.76–46.28		1.01–2.00	1.12–2.00	0.11–0.50

Table 5 Melting range, coefficient of thermal expansion and average variation of density of experimental 18K alloys

Alloy	**Type**	**d_{RT} [$g{\cdot}cm^{-3}$]**	**$CTE_{a(sol\text{-}liq)}$ [$10^{-6}\ K^{-1}$]**	**d_{sol} [$g{\cdot}cm^{-3}$]**	**d_{liq} [$g{\cdot}cm^{-3}$]**	**$\Delta d_{RT\text{-}sol}$ [$g{\cdot}cm^{-3}$]**	**$\Delta d_{sol\text{-}liq}$ [$g{\cdot}cm^{-3}$]**	**$\Delta d_{RT\text{-}liq}$ [$g{\cdot}cm^{-3}$]**
A	Au	19.32	17.25 -64.73	18.313	17.298	0.987	1.015	2.002
B	Au Cu 51 at.%	14.69	20.87 – 72.17	13.974	13.711	0.716	0.263	0.979
C	AuCu Zn 2 at.%	14.75	20.27 – 72.15	14.055	13.711	0.694	0.344	1.038
D	AuCu Ge 2 at.%	14.60	19.56 – 71.87	14.019	13.279	0.581	0.741	1.322
E	AuCu Si 0.5 at.%	14.71	19.59– 74.64	14.063	13.160	0.647	0.903	1.550
F	AuCu Ag 2.0 at.%	14.81	20.04 – 72.78	14.114	13.671	0.696	0.443	1.139
G	AuCu Zn 2.0 at.% Ge 2.0 at.%	14.68	19.52 – 71.23	14.116	13.393	0.564	0.723	1.287
H	AuCu ZnGe2at.% Si 0,5%at	14.64	19.68 – 73.85	14.093	13.215	0.547	0.878	1.425

Table 6 Variation of density percent change of experimental alloy respect to room temperature

ALLOY	**d_{RT} [$g{\cdot}cm^{-3}$]**	**$\Delta d_{\%RT\text{-}sol}$ [$g{\cdot}cm^{-3}$]**	**$\Delta d_{\%sol\text{-}liq}$ [$g{\cdot}cm^{-3}$]**	**$\Delta d\%_{RT\text{-}liq}$ [$g{\cdot}cm^{-3}$]**
Au	19.32	5.11	5.26	10.37
B	14.69	4.87	1.79	6.66
C	14.75	4.71	2.33	7.04
D	14.60	3.98	5.07	9.05
E	14.71	4.40	6.14	10.54
F	14.81	4.70	3.00	7.69

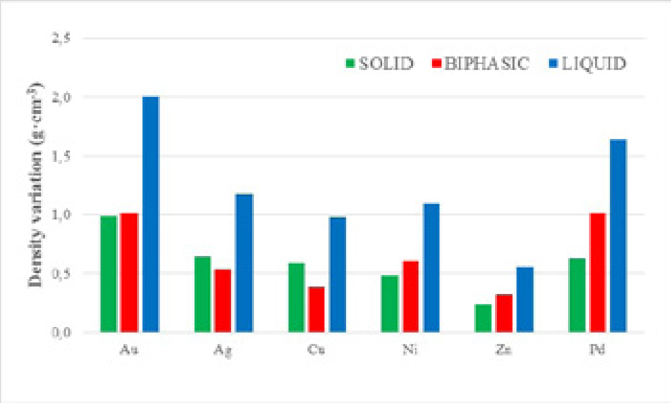

Figure 7 Density variation of the 18K experimental alloys as a function of their physical state

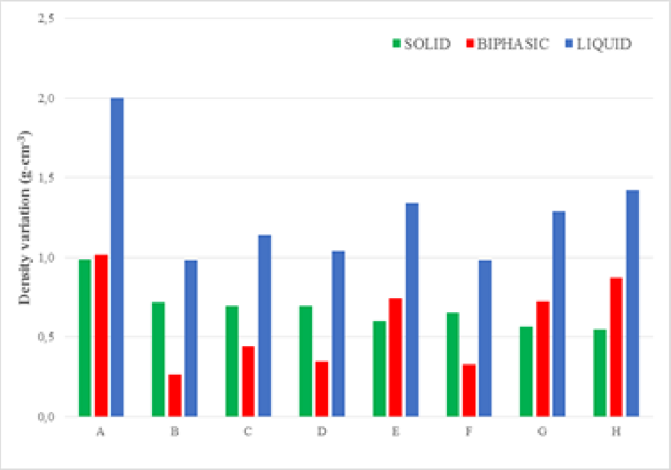

Figure 8 Density variation of the 18K experimental alloys as a function of their physical state

G	14.68	3.84	4.93	8.77
H	14.64	3.84	6.00	9.84

The experimental alloys were obtained with the addition of copper to pure gold (A) and a single modifying element in one of the most common karat gold matrix (B-F, Au 18K) in order to study in a more systematic manner the effect of each element on form-filling and density variation in the melting range. The compositions were made by the addition of 2 at.% of more soluble elements: Ag (F), Zn (C), Ge (D) , and the addition of 0.50 at.% of the less soluble one, Si (E), and some of their combinations (G-H).

The simplest binary matrix (B) has shown a density change across the melting range distinctively lower ($\Delta d_{sol\text{-}liq}$ = 0.263 g/cm^3) than the density change of pure copper ($\Delta d_{sol\text{-}liq}$ = 0.384 g/cm^3), which is the element with the lowest value. This phenomenon could be due to a relevant lattice distortion induced by copper at high temperature; indeed, its density at the solidus temperature is relatively lower compared to those of other experimental alloys (d_{sol} = 13.974 g/cm^3).

The ternary alloy with 2 at.% germanium (D) or with 0.5 at.% silicon (E) showed the highest density change during melting, 0.741 g/cm^3 and 0.903 g/cm^3, respectively. They were followed by the alloys containing 2 at.% silver (F) (0.443 g/cm^3) and 2 at.% zinc (C) (0.344 g/cm^3). The silicon addition (Si) is the one that imparts the smallest change of density with respect to the liquid state, but it should be noticed that its atomic fraction is four times lower. The total changes of density from room temperature to the liquid state follow the same trend of variations determined in the melting range (Figure 7), while the variations in the solid state are roughly the same.

With the experimental quaternary and quinary alloys, the density change across the melting range is higher on average, equal to 0.723 g/cm^3 for the germanium and zinc-containing alloy and 0.872 g/cm^3 for the alloy having zinc, germanium and silicon. This aspect reveals the possible interactions among these elements and the cumulative effect as a function of their bond nature and atomic fraction. It is relevant noticing that in the presence of germanium and silicon, the density changes during the melting range are always greater than those at the solid state, contrary to what occurs for other alloys (Figure 8).

In the dilatometric curves, the shift of the order-disorder transition with respect to the gold-copper matrix is noteworthy (Figure 9). The presence of germanium or silicon (Alloys D, E, G and H) seems to lower the beginning of this transformation by about 80°C (144°), while silver and zinc seem to have a negligible effect. The order-disorder transformation results in the formation or disruption of intermetallic phases having a more regular and compact structure (AuCu). Thus, in the temperature range where these compounds' phases form (230–410°C/ 446–770°F), a temporary increase of density occurs. At higher temperatures, these intermetallic compounds are no longer stable and they dissolve into the structure metallic matrix, giving way once again to a linear behavior of density until the beginning of the melting.

The final set of materials studied represents alloys with compositions similar to classical jewelry in several gold assayings, namely true commercial-like (like commercially available) alloys (Table 7). The 18K group has shown an average density change

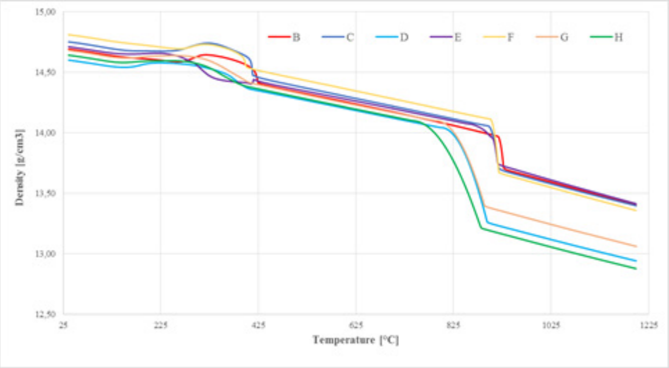

Figure 9 Density of experimental alloys (18k) as function of temperature respect to matrix alloy (B)

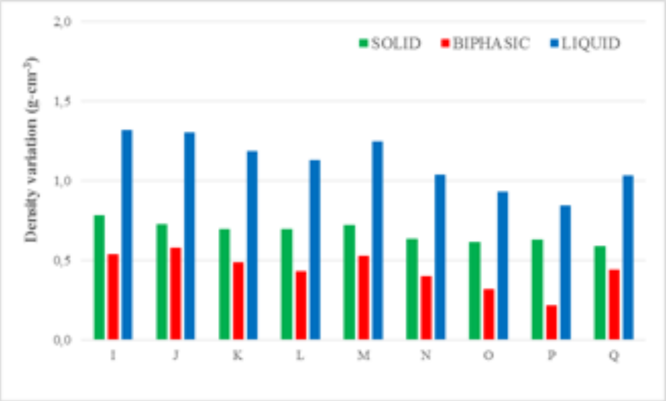

Figure 10 Variation of density of some commercial alloys as a function of their physical state

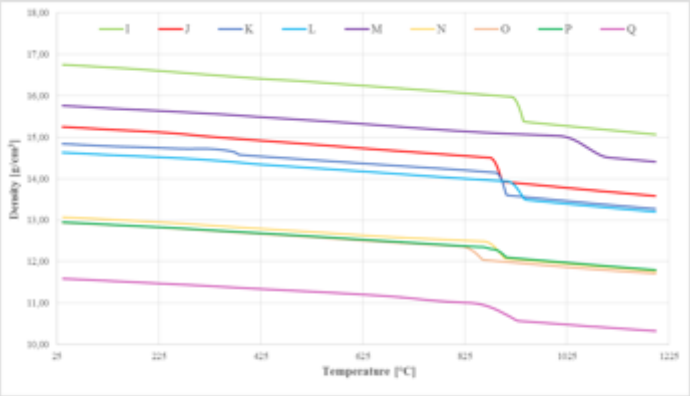

Figure 11 Full range density variation as function of temperature and gold assay for commercial-like alloys

across the melting range ($\Delta d_{sol\text{-}liq}$) of approximately 0.51 g/cm³ (Figures 10 and 11) and a change of about 0.71 g/cm³ in the heating stage from room temperature to solidus temperature ($\Delta d_{RT\text{-}sol}$). This provides a total average density change from room temperature to liquidus temperature of $\Delta_{RT\text{-}liq}$ = 1.22 g/ cm³ (Tables 8 and 9). The change of density in the solid state seems to be nearly 30% higher with respect to that determined during the phase transition from solid to liquid, and this could be attributed to the relevant presence of copper and silver. The yellow-gold alloy (J) shows a higher change of density ($\Delta d^{sol\text{-}liq}$) during melting, probably because of the lower content of copper. For the red alloy (K), whose copper content is distinctly higher, the change of density is lower and the resulting values stand between those of yellow gold (J) and white nickel alloy (L) in 18K. In the temperature range of 200–400°C (392–752°F), the curve for onset of density due to order-disorder transformation is clearly appreciable for the 18K red gold (K). The behavior of nickel white-gold alloy (L) is also very interesting because its density variations in the melting and full range of temperatures were quite a bit lower than the density changes of yellow and red 18K alloys. This was quite unexpected in view of the high density change in pure nickel during melting. Indeed, stone-in-place casting with white-nickel alloys are more prone to stone cracking after flask quenching, but this mainly occurs for higher yield strength (+100 MPa) and lower ductility relative to yellow and red 18K golds.

Table 7 Weight and atomic percentage of commercial alloys in various fineness

Alloy	Au [wt.%] [at.%]	Cu [wt.%] [at.%]	Ag [wt.%] [at.%]	Ni [wt.%] [at.%]	Pd [wt.%] [at.%]	Zn [wt.%] [at.%]	Deox	Refiner	Others
I	87.50 70.93	10.12 25.43	2.25 3.33			0.13 0.32		√	
J	75.00 54.55	12.75 15.61	11.75 28.75			0.50 1.10		√	
K	75.00 50.25	21.75 45.17	2.50 3.06			0.75 1.51		√	
L	75.00 48.67	14.00 28.16		7.50 16.33		3.50 6.84	√	√	
M	75.00 55.99	9.85 22.98			13.07 18.06			√	Ga, In
N	58.50 32.95	33.60 58.66	7.50 7.71			0.40 0.68		√	
O	58.50 33.23	27.00 47.55	8.30 8.61			6.20 10.61		√	
P	58.50 32.47	34.80 59.86	5.20 5.27			0.50 0.84	√	√	Ga
Q	41.70 19.95	47.20 70.01	10.50 9.17			0.60 0.86		√	

Table 8 Fusion range, average thermal expansion coefficient and average density change according to the physical state

Alloy	TYPE	$\Delta T_{sol\text{-}liq}$ [°C]	d_{RT} [g·cm⁻³]	$CTE_{a(sol\text{-}liq)}$ [10^{-6} K^{-1}]	d_{sol} [g·cm⁻³]	d_{liq} [g·cm⁻³]	$\Delta d_{RT\text{-}sol}$ [g·cm⁻³]	$\Delta d_{sol\text{-}liq}$ [g·cm⁻³]	$\Delta d_{RT\text{-}liq}$ [g·cm⁻³]
I	RG 21KT	920-940	16.77	18.28–70.17	15.988	15.452	0.782	0.536	0.536
J	YG 18KT	876-885	15.25	19.47–76.10	14.525	13.945	0.725	0.580	0.580
K	RG 18KT	891-899	14.84	19.26–74.37	14.145	13.657	0.695	0.488	0.488
L	WG 18KT	909-939	14.63	18.94–76.90	13.935	13.503	0.695	0.432	0.432
M	WG 18KT	1009-1079	15.76	16.20–66.68	15.041	14.514	0.719	0.527	0.527
N	RG 14KT	867-902	13.07	18.46–78.10	12.434	12.033	0.636	0.401	0.401
O	YG 14KT	824-865	12.94	19.87–70.31	12.358	12.041	0.612	0.317	0.317

P	RG 14KT	856-905	12.95	19.74–77.43	12.348	11.966	0.602	0.382	0.382
Q	RG 10KT	838-922	11.64	22.07–78.75	11.049	10.609	0.591	0.440	0.440

Table 9 Percent change of density of commercial-like alloys respect to room temperature

ALLOY	**d_{RT} [g·cm^{-3}]**	**$\Delta d\%_{RT\text{-}sol}$ [g·cm^{-3}]**	**$\Delta d\%_{sol\text{-}liq}$ [g·cm^{-3}]**	**$\Delta d\%_{RT\text{-}liq}$ [g·cm^{-3}]**
I	16,77	4,663	3,196	7,859
J	15,25	4,754	3,803	8,557
K	14,84	4,683	3,288	7,972
L	14,63	4,751	2,953	7,703
M	15,76	4,562	3,344	7,906
N	13,07	4,866	3,068	7,934
O	12,94	4,497	2,450	7,179
P	12,95	4,649	2,950	6,510
Q	11,64	5,077	3,780	8,857

Even though the weight percentage of gold is notably higher when compared to other elements due to its elevated density (19.32 g/cm^3), its atomic concentration,
which determines the real behavior of the alloy, is considerably lower and almost identical to the atomic fraction of copper (Table 7). The palladium white-gold alloy (M) has an average density change very similar to that of red-gold alloy (K) (Figure 10).

The red-gold alloys 14K (N-P) showed density changes that were on average lower (ΔdRT-liq = 0.99 g/cm^3) compared to 18K alloys (Figure 10), notwithstanding the fact that their initial density is lower. This smaller change of total density is caused by a simultaneous smaller average change of density across the solid state ($\Delta d_{RT\text{-}sol}$ = 0.62 g/cm^3) and the smaller average density change across the melting range ($\Delta d_{sol\text{-}liq}$ = 0.37 g/cm^3). The smaller density change compared to higher karat alloys (18K) could imply advantages in terms of lower volume modification for some products, probably lower shrinkage porosity and a reduction of internal stresses that are consequences of solidification and the compression of the stones set in the wax patterns, which consequently will be less prone to breaking. Smaller size variations between the liquid and solid phase can thus allow obtaining a better correspondence between the jewelry project and the production result, besides guaranteeing a faster production process and greater toughness. Ideally, the value of density of alloys at the liquid state should stay unaltered compared to the density at the solid state.

Furthermore, the comparison of the resulting dilatometry analysis of a 14K alloy containing an expansive element, gallium, whose density in the liquid state is higher than in the solid state (P), and an analogous alloy that does not contain such an element (P*) sheds light on the effect these types of additives can produce. The alloy that does not contain gallium shows a density change during the melting range that is about 20% higher than the density variation of the alloy with gallium. The density changes in the solid state are almost identical (Table 10).

Table 10 Melting range, CTEa and density changes of 14K alloys with and without gallium

Alloy	**TYPE**	**$\Delta T_{sol\text{-}liq}$ [°C]**	**d_{RT} [g·cm^{-3}]**	**$CTE_{a(sol\text{-}liq)}$ [10^{-6} K^{-1}]**	**d_{sol} [g·cm^{-3}]**	**d_{liq} [g·cm^{-3}]**	**$\Delta d_{RT\text{-}sol}$ [g·cm^{-3}]**	**$\Delta d_{sol\text{-}liq}$ [g·cm^{-3}]**	**$\Delta d_{RT\text{-}liq}$ [g·cm^{-3}]**
P	RG 14KT	856–905	12.95	19.36 – 77.53	12.348	11.966	0.602	0.382	0.984

P*	RG 14KT	876–914	12.97	19.34 – 75.33	12.367	11.907	0.603	0.460	1.063

A classical lower fineness alloy (Q) evidenced once again a total variation of density significantly higher ($\Delta d_{RT\text{-}liq}$ = 1.03 g/cm^3), very similar to that of high fineness alloys (I) that showed a variation of density equal to 1.32 g/cm^3 (Figure 11).

The low karat (10K) gold alloy (Q) showed an increase in the density change ($\Delta d_{sol\text{-}liq}$ = 0.44 g/cm^3) during the melting range compared to alloys in 14K ($\Delta d_{sol\text{-}liq}$ = 0.40 g/cm^3), even though the content of copper is higher. This goes against the concept that the variation of density of the main element (Cu) between the solid and liquid phase could explain the smaller density changes of the 14K alloys when compared to 18K alloys.

A possible explanation for this higher density change in the melting range for lower karat alloy (Q) is that it presents a wider melting range than the 14K alloy (N). In practice, since the less noble alloy starts to solidify 20°C before and completes the solidification 30°C after alloy (N), the material has more chance to change its density. This advantage is then counterbalanced by the fact that the solidification temperature of lower karat alloy (Q) is closer to room temperature and the density change during complete cooling is smaller. In the solid state, however, the opposite phenomenon takes place. The density change is higher for the alloy with higher fineness and the resulting total density change is identical for both alloys.

The average coefficient of thermal expansion (CTE_a) of 18K gold alloys is similar to that of pure copper. The only exceptions are white golds with a high content of palladium (M), for which this coefficient is very similar to that of pure gold. In fact, pure palladium has a thermal expansion coefficient similar to pure gold. This means that objects in white gold with a high content of palladium tend to preserve their geometry better if subjected to heating. In addition, they tend to change their density less. If total shrinkage of the molten mass is the only consideration, it is less harmful to increase the superheat of a white gold containing palladium than a yellow gold while trying to improve the filling in the narrower channels. However, the higher temperature increases the risk of thermal mold decomposition.

A very interesting aspect derives from the fact that the coefficient of thermal expansion of one alloy $CTE_{a\,(alloy)}$ seems to be a weighted average of the thermal expansion coefficients of the elements constituting the material by their atomic fractions (Table 11). In practice, it is possible to predict the coefficient of thermal expansion for any alloy $CTE_{a(alloy)}$ starting from the atomic composition of the pure elements (x_i) and their coefficient of thermal expansion and obtain a percent difference within 10% of experimental values (Equation 1). This rule seems to be valid even at the liquid state. The knowledge of the average coefficients of thermal expansion is very useful, especially during the soldering process because it allows one to estimate the stress that is applied to the solder alloy after the joint is made. This is particularly true for low-karat gold alloys, where stress-corrosion and failure phenomenon can take place.

$$CTE_{a(alloy)} = \sum_{i=1}^{N} x_i \cdot CTE_{a(i)}$$

(Equation 1)

Table 11 Calculated and experimental coefficients of thermal expansion for gold alloys

Alloy	**CTE$_{a(sol\text{-}liq)}$ [10^{-6} K^{-1}]**	**CTE$_{a(teor.)}$ [10^{-6} K^{-1}]**	εr [%]
I	18.28	18.46	1.01
J	19.47	19.78	1.58
K	19.26	19.45	1.00
L	18.94	19.17	1.20
M	16.20	17.31	6.86
N	18.46	20.04	8.54
O	19.87	21.92	10.3
P	19.74	20.01	1.38
Q	22.07	20.58	6.76

Form-Filling

The castability of gold alloys was studied not only on the basis of density change from solid to liquid, but also with respect to the ratio of characteristic temperatures of the alloys that determine the melting range. In the past, some studies have been carried out to determine the influence that the casting temperature (T_C), the solidus temperature (T_S) and the mold temperature (T_M) have on the indirect form-filling or castability index of the patterns ($C_{V,t}$) through the use of equations.
In order to take into account the differences between the alloys, these equations apply two constants (a, b), that are specific to each alloy (Equation 2). However, these studies were mainly directed towards alloys that are used in dentistry.[7] On the other hand, this study was an attempt to provide operators in the jewelr industry a more practical and direct tool able to estimate, at least qualitatively, the castability index of a given precious alloy based only on the content of elements that can substantially modify the densities as a function of the physical state and the characteristic melting temperatures, in particular the solidus temperature.

$$C_{V,t} = a + b \cdot \frac{T_M^2}{\sqrt{(T_C - T_S)}}$$

(Equation 2)

In this study the casting temperature of an alloy was set to approximately 100°C (180°F) above the liquidus temperature, so that the number of variables affecting the system was reduced. This was acceptable considering that in industrial practice the casting temperature varies only slightly compared to the mold temperature. Usually, the casting temperature varies only a little around an advisable average value ($T_C = T_{liq}+100°C$) while the temperature of the molds can vary up to ±100°C with respect to the average commonly suggested value of around 650°C. The mold temperature is mostly related to the items' thickness and, in our case, was fixed at this average value, 650°C. The mass of the casting was kept constant at 175 grams.

The analysis was performed in a similar way to the dilatometry. It started with the study of the pure gold matrix (A in Table 4), to which single alloying elements were subsequently added before continuing with a more complex combination of the same elements. The first addition of copper (51 at.%) is necessary in order to achieve an 18K gold alloy, but this addition does not significantly modify the melting range. Then, different concentrations of additives were made to the goldcopper matrix with the aim of substantially modifying the melting range. In this way the contribution of each single element towards form-filling (or castability index) was determined before considering their interaction in more complex alloys, since there could be interaction effects that could cause deviations from simple linearity. The additions of these elements were calculated in atomic percentage because the intensity of their effects depends on the concentration in which the atoms are distributed within the gold matrix.

Additionally, the form-filling or castability index was also studied as a function of the perforations in the steel flasks (see Figure 13) containing the investment mold because the presence of an inadequate porosity along their surface restricts the ejection of casting gas inside the cavities and can hinder form-filling. In this manner, it is possible to discern between an insufficient form-filling due to the lack of mold porosities and an insufficient form-filling given by the characteristic temperatures of the alloy and its variation in density during solidification, besides the influence of other properties that now are not taken into account. In theory and in the same conditions, a large open area in wall perforations should provide a better form-filling index ($C_{V,t}$). In a similar way, at the same conditions and perforation degree of the flask wall, an alloy with a wider melting range should provide better filling.

A flask's perforations can go from zero (f = 0.00%) to a maximum ideal value in which each hole is tangent to the others (f = 90.69%). However, in this last case the mechanical properties and durability of the flasks could rapidly worsen because the cyclic thermal dilatation and shock under quenching, together with the continuous oxidation of the metal over time and the flask tong loads, could cause a fast rupture. Indeed, the proposed maximum perforations amount can be evaluated based on the typical permeability of the investment mold after burnout, whose value is around 50 vol.%.12,13 The perforation area of the flasks can be considered as a form of porosity or permeability and hence it is sufficient to obtain a perforation level equivalent to the value of porosity of the investment molds in order to avoid additional resistance from the flask wall during degassing. The presence of wall perforations ensures a more efficient removal of the entrapped gas inside pattern cavities, known in the metallurgical field as back-pressure effect, because it improves the permeation and escape of gases during casting. These gases derive principally from the incomplete vacuum in the casting chamber, from the partial decomposition of the investment, from the desorption of dissolved gas inside the molten metal during solidification, and from the permeation of argon coming from the crucible.

By definition, the maximum purposeful degree of perforations can be considered equivalent to the porosity of the investment molds. Moreover, the volume and the surface porosities in the same material are not numerically equal, and changing from one to the other requires a conversion factor to go from space to surface parameters. In the hypothesis that porosity is perfectly spherical, uniform and interconnected, similar to the position of atoms in a closed-packed lattice (Figure 12), the maximum volume of porosity corresponds to the fraction of volume occupied

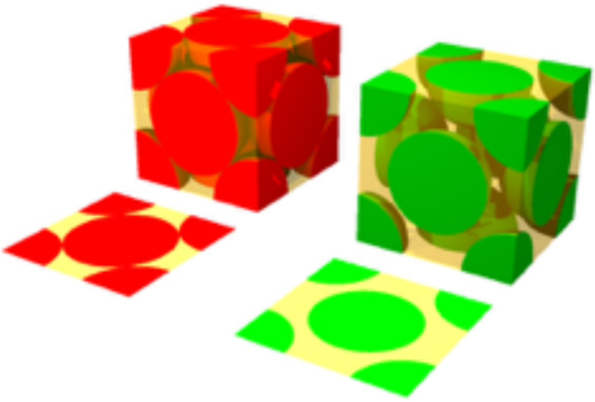
Figure 12 Maximum and typical theoretical volume and surface porosity

Figure 13 The series of cylinders with different perforation degrees for the study of castability

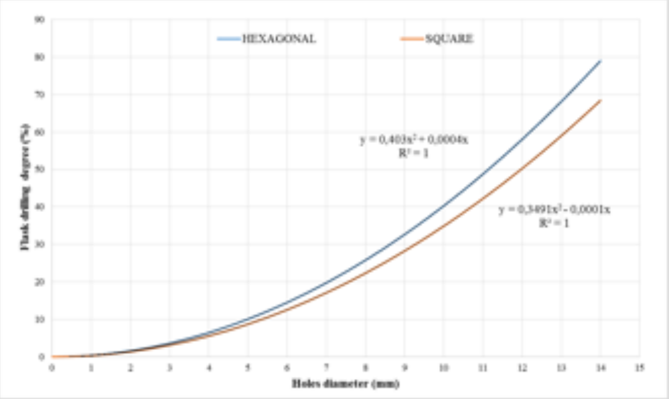

Figure 14 Degree of porosity as a function of the opening diameter

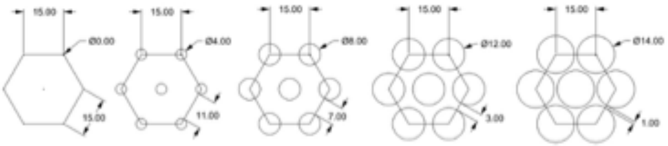

Figure 15 Hexagonal structures for different perforation degrees

by the spherical cavities inside a cube (74.0 vol.%) while the maximum surface porosity corresponds to the fraction of area occupied by the circles along a cube face (78.5 vol.%). In other words, the value of porosity on a surface is numerically higher than the value of volume porosity. In real conditions, the section of a solid cut perfectly in half does not expose all the internal porosities, nor will all porosities be connected. However, this consideration allows an estimation of the maximum value of surface porosity that is found on the surface of a uniform porous solid such as investment. Consequently, the maximum value of porosity also allows one to estimate the best perforation degree of the flask walls. Given the hypothesis that volume porosity of the refractory molds fired through a traditional burnout cycle is about 50%, then the perforations of the flask walls should be around 61% in order to ensure the maximal theoretical degassing effect.

The perforation degrees of the flasks were chosen in such a way that permeability for a typical investment mold after burnout is included in the range (Figure 13).

The open area caused by perforations in the wall of a flask is a function of hole size and shape (Figure 14). This is the reason why the hexagonal compact structure was favored for the study of the influence that the flask perforations have on the castability of the alloys. The simulation was carried out imposing a constant center distance of 15 mm between all openings, an average value that is commonly used in flask production. The porosity as a function of the diameter depends on this parameter as well.

The phenomenon of the back-pressure also depends on the amount of porosity in the investment mold and not only on the perforation degree of the containing flasks. In general, the level of porosity of the mold depends on the starting particle size distribution of the investment powder, on the water:powder ratio employed and on the burnout cycle.[11] A higher open porosity of the flask implies a reduced resistance to the escape of the casting gases, a lower resistance of the molten flux and a better filling of the patterns. The only method to modify the permeability of the gases through the walls of the flasks, given that the raw materials and the process conditions are always the same, is to modify the perforation area of the flasks used to contain the investment mold.

However, the form-filling degree of the patterns does not only depend on the resistance given by the back-pressure, but also on the composition of the alloy, thus the use of certain cylinders with small perforations can be compensated for by using alloys with a high form-filling performance. In some instances, the use of a flask with a low opening area or even without holes can be advantageous in certain applications, i.e., casting with stones in which quenching has to be done in air for long periods of time and a closed flask wall hinders the permeation of air towards the hot tree and, consequently, also its oxidation. In these cases, an alloy with a high form-filling performance and a lower melting temperature could be an adequate solution.

Five types of flasks with hexagonal holes were studied. The diameter of the holes was four, eight, twelve and fourteen millimeters, respectively, and one flask that did not possesses openings of any type (Figure 15). These perforations

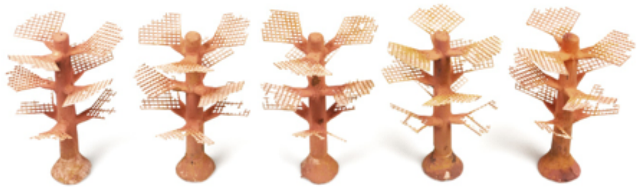

Figure 16 Alloy (K) trees from gravity casting and in order of increasing flask hole diameter

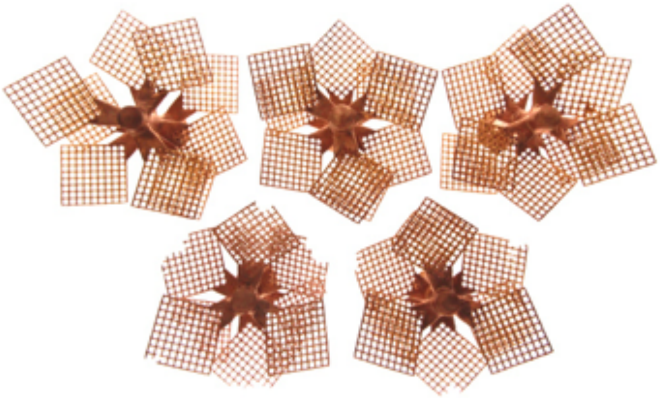

Figure 17 Alloy (K) trees from pressure-assisted casting in counterclockwise increasing order of flask hole diameter

correspond to a surface porosity of the flasks that goes from 0% to about 80% of the total wall surface available.

The castability index or direct form-filling (C_V) is determined from the weight ratio between the total mass of the cast grids (Figures 16 and 17) and the ideal mass that grids would have if they were completely filled (Figure 3). The average weight of a single grid is 0.2213 ±0.0045 g of wax (d_{wax} = 0.934 g/cm^3). The castings were performed using simple gravity and casting aided by overpressure and suction of the molten alloys inside the molds in order to compare the results obtained with both methods. The alloy chosen for these first tests was an 18K red gold (K) ($T_{liq.}$ = 899°C/1650°F), cast at 1000°C (1832°F) with three argon purging cycles and a thirty-second homogenization before pouring. In the test aided with pressure, the flask chamber vacuum was set at -1.0 bar while the molten alloy was pressurized at +0.5 bar immediately after the crucible emptied from the crucible chamber. The flask temperature was set at 650°C (1202°F).

In the case of gravity casting, the form-filling of the trees was very similar (Table 12), independent of the flask perforations (Figure 16), and it is equal to about 60% of the potentially available mass for the complete grids. The grids at the top of the casting trees tend to be more filled because of the higher fluid-dynamic energy of the molten alloy, while the grids at the bottom are markedly less complete. The fact that the opening degree does not influence the castability of the alloy during gravity casting means that in these conditions the energy of the molten mass does not overcome the backpressure given by the casting gas and the superficial tension of the liquid alloy.

Table 12 Grids weight obtained through gravity casting of alloy (K) as a function of flask hole diameter

ELEMENT	Ø 0 mm [g]	Ø 4 mm [g]	Ø 8 mm [g]	Ø 12 mm [g]	Ø 14 mm [g]
Top	2.653 2.362 3.130	2.718 2.633 2.852	2.806 2.717 2.874	2.932 2.877 2.910	2.550 2.778 2.682
Center	2.650 2.677 2.779	2.621 2.880 2.683	2.355 2.082 2.311	2.208 2.201 2.378	2.720 2.272 1.874
Bottom	1.183 1.192 1.240	1.208 1.710 1.712	1.302 0.789 1.052	0.951 1.118 1.400	1.375 1.064 1.319
Filling (%)	62.80 ±7.16	66.44 ±5.81	57.81 ±7.24	59.98 ±7.14	58.90 ±8.05

Table 13 Grids weight obtained with vacuum casting of alloy (K) as a function of flask hole diameter

ELEMENT	Ø 0 mm [g]	Ø 4 mm [g]	Ø 8 mm [g]	Ø 12 mm [g]	Ø 14 mm [g]
Top	3.342 3.109 3.475	3.228 3.293 3.345	3.435 3.386 3.281	3.321 3.379 3.067	3.299 3.201 3.147
Center	3.078 2.855 2.882	3.102 3.261 3.037	3.380 3.432 3.325	3.217 3.260 3.114	3.481 3.288 3.194
Bottom	2.404 2.274 2.294	3.028 3.052 3.278	3.354 3.308 3.342	3.409 3.239 3.258	3.281 3.330 3.177
Filling (%)	81.28 ±4.60	90.48 ±2.72	95.60 ±2.66	92.51 ±2.73	92.93 ±2.71

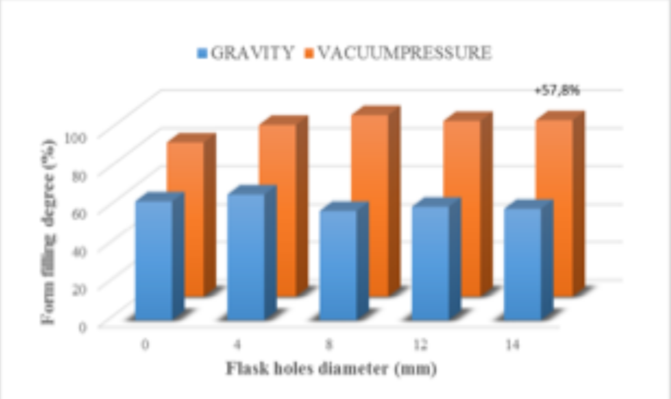

Figure 18 Filling percentages as a function of the opening diameter and the type of casting

A very interesting aspect is given by the fact that even if the grids seem visibly filled (Figure 17) during vacuum casting, from a numerical point of view the average form-filling percentage is only about 95% (Table 13). This fact can be attributed to the presence of micro-porosity inside the solidified material or to the stretching that the alloy undergoes in the grid channels during the last phase of solidification. The areas of the grids that are more distant from the ingate are indeed thinner and rounder at the edges and this means a reduction of material compared to the quantity that the pattern could theoretically accumulate, even if the general aspect of the cast grids looks complete (Figure 18).

$$C_V{}^{1.5\text{bar}} = k_{1.5\text{bar}} \cdot C_V^{g}$$

(Equation 3)

In the case of closed wall flask (D = 0.00 mm) and smallest holes (D = 4.00 mm), it is possible to derive an empirical relationship (Equation 3) between form-filling for gravity ($C_V^{g)}$ and pressure-assisted casting (C_V^{P}). The suction of the molten alloy (P_{vac} = -1.0 bar) into the flask and its pressurization with protective gas (P_{comp} = +0.5 bar) from the crucible side act in a subsequent and cumulative way, accounting for a total pressure of 1.5 bar. Indeed, a suction effect operates from the early moments of pouring, while gas compression starts at the end of pouring alone, but they both participate in form-filling. The suction improves the filling into the tree head and the gas pressure allows the completion at the bottom of the tree to compensate for the total energy loss of the molten alloy. The vacuum pressure-assisted technique enhances over gravity form-filling by approximately 30% (k = 1.33 ±0.03), but in the case of flasks with large perforations, this enhancing effect is considerably greater (k = 1.54 ±0.06) but more difficult to determine with accuracy because the form-filling percentages were already near completion. Indeed, as expected, the enhancing factor (k) arising from the vacuum pressure technique is not constant in all conditions, but it is a function of the pressure values triggered in the casting machine. In the case of experimental materials, pure gold casting has shown a very high form-filling (72.56%), higher than most of the alloys. Alloying other elements to the gold reduces the form-filling ability (Table 14).

The form-filling of pure copper and pure silver was also verified since these two elements, along with gold, constitute most of the precious metal alloys. Silver showed a form-filling even higher than that of gold, while copper showed the lowest filling even when compared to some of the other alloys. Molten copper has a higher surface tension than molten gold, which, in turn, is higher than silver. This trend could explain the observed form-filling characteristics of these metals.[14]

The poor form-filling of pure copper could be the reason for the low gridcompletion values in the gold-copper alloy (B, 67.01%). This form-filling degree seems to be in line with the value expected after calculating the total variation between pure gold (A) and pure copper (Table 14). The highest form-fillings also seem to belong to the elements exhibiting the largest density changes during solidification. The comparison between copper and gold is even more direct, because their melting temperature is almost identical. In the case of silver, a lower melting point has to be taken into account (961°C/1762°F) because it is closer to mold temperature (650°C) and, therefore, the cooling rate of the molten alloy is slower. This can overcome the minor density variation at the melting point. Furthermore, the gold-copper matrix (18K) with single modifying element (C–E) that increases the melting range in the concentrations of 2 at.% for zinc, germanium and 0.5 at.% for silicon, demonstrates unexpected form-filling values as evidenced from previous works.[7]

Table 14 Grid weights obtained by gravity castingas a function of experimental alloys (A-H)

POSITION	A	B	C	D	E	F	G	H	Ag	Cu
Top (g)	4,234 4,354 4,396	2,610 2,706 2,696	2,496 2,839 2,787	2,518 2,565 2,560	2,494 2,546 2,451	2,536 2,458 2,727	2,719 2,524 3,037	3,102 3,322 3,332	2,149 2,277 2,114	1,598 1,631 1,522
Center (g)	3.078 2.855 2.882	2,370 2,301 2,463	2,525 2,655 2,476	2,178 2,246 2,193	2,018 2,144 2,496	2,737 2,494 2,472	2,673 2,497 2,353	2,799 2,683 2,951	2,126 2,161 2,140	1,279 1,299 1,500
Bottom (g)	2.404 2.274 2.294	2,100 1,753 1,986	1,592 1,247 1,241	1,923 1,777 2,028	1,017 1,425 1,170	2,336 2,228 2,169	1,608 1,843 2,084	1,890 2,105 1,591	1,878 1,850 1,749	0,886 0,772 0,828
Filling (%)	72,56 ±3,38	67,01 ±1,06	63,07 ±2,10	64,22 ±0,92	56,64 ±1,96	70,18 ±0,63	67,90 ±1,44	76,18 ±2,04	82,48 ±0,80	59,64 ±1,81

At the same time, the ternary alloy containing germanium (D) presented the highest variation of density over the melting range (0.741 g/cm^3), which means that during the passage from solid to liquid, it experiences a higher volumetric contraction. This is in line with the initial hypothesis that establishes that a higher variation of density promotes form-filling (Figure 7). This starting data is then further confirmed by the behavior of 18K ternary alloys containing silicon or zinc.

The ternary alloy containing zinc (C) shows a smaller variation of density in the melting range (0.344 g/cm^3), and thus filling turns out to be less (63.07%) compared to the alloy containing germanium. The ternary alloy containing silicon (E) seems to be an exception because, with its high density reduction in its melting range (0.903 g/cm3), it should provide a highly fluid melt, but silicon alone probably increases other relevant factors such as viscosity and surface tension, leading to significant form-filling reduction (56.64%).

In these concentrations, additives do not seem to improve the form-filling, yet alloys that exhibit greater density change over the melting range reduce the filling less, if compared to pure gold. Consequently, ternary alloys containing germanium reduce filling less than ternary alloys containing zinc, but there can be substantial deviations as in the case of silver (F) that provides a relatively high form-filling (70.18%), though the alloy density variation into melting range is smaller and the melting temperature is quite higher at the same atomic concentrations. However, there seems to be a connection between density variation in the melting range and the form-filling capability of an alloy, namely the castability inside the patterns. A further confirmation of this hypothesis is given by the high filling obtained (76.18%) with a quinary complex alloy containing zinc, germanium, and silicon (H), which also presents the highest density change across the melting range.

Finally, the influence of grain refiners on form-filling was examined, since in the literature little information other than hypothetical trends was found. Two almost identical alloys, differing only by the presence or absence of grain refiner, were

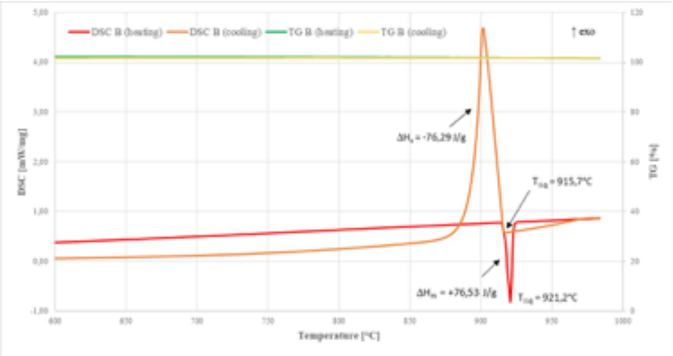

Figure 19 Heating and cooling run for 18K matrix alloy (B)

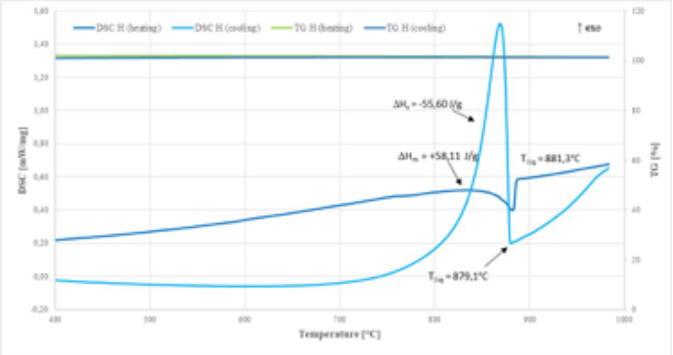

Figure 20 Heating and cooling run for 18K matrix alloy (H)

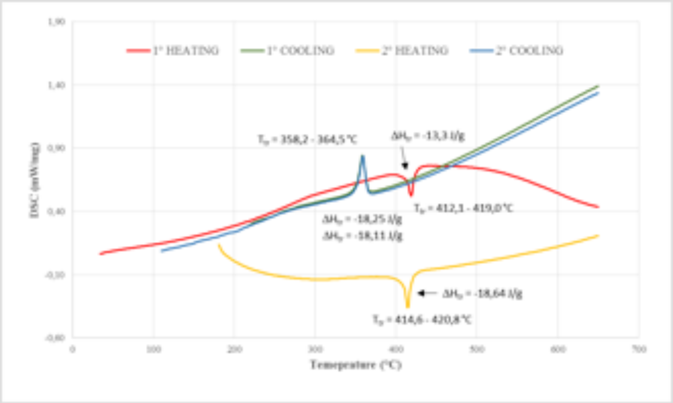

Figure 21 DSC of AuCu equimolar alloy (Au 50 at.%, Cu 50 at.%)

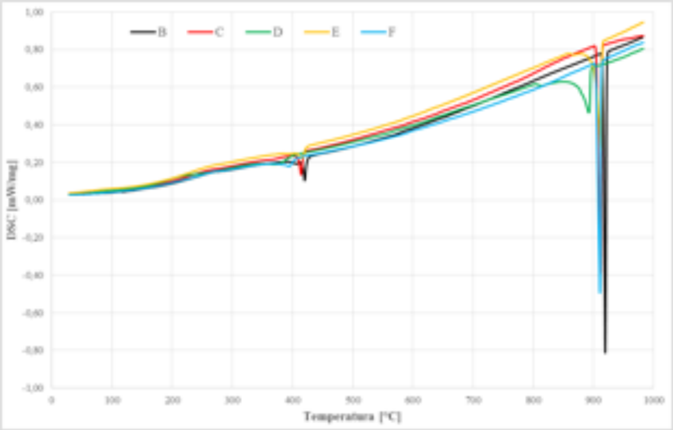

Figure 22 Differential scanning calorimetry (DSC) of ternary alloys respect to AuCu matrix

cast under the same conditions and using the same grid patterns in order to compare the form-filling of both alloys. Using as a reference the flask with 12 mm openings, the percent of form-filling of the alloy without grain refiner (59.40 ±8.05%) was only about 0.60% less compared to the alloy containing the grain refiner (59.98 ±2.46%). From a technological point of view, therefore, it is difficult to affirm that in such conditions the grain refiner has a significant role in the form-filling of the patterns.

DIFFERENTIAL SCANNING CALORIMETRY

The energy required to melt a solid material is directly related to the thermodynamic quantity named enthalpy of fusion (J/g). Melting is an endothermic process because energy must be given to the material in order to break stable chemical bonds. In the case of single elements, the melting process is displayed as a sharp peak in the energy signal (DSC) because pure metals melt at a single precise temperature. In the heating and melting process, it is likewise important to monitor the mass transformation of the specimens in order to control for dangerous composition changes, and this can be provided by thermogravimetric signal (TG). A traditional thermal analysis is given for gold-copper matrix (B) and the more complex experimental alloy (H) containing zinc, germanium and silicon (Figures 19 and 20). The thermogravimetric curves did not show any peculiar mass transformation of the materials, so it was possible to examine the energetic signal in a more reliable manner.

In the gold-copper matrix (B), the melting process requires about +76.53 J/g, which are released in a very symmetrical way during solidification (-76.29 J/g). The liquidus point during heating is placed around 921.2°C (1690.2°F) and at about 915.7°C (1680.3°F) during cooling, providing just a little undercooling for solidication (4.5°C/8.1°F).

The recorded enthalpies for pure gold and silver are close to those reported in literature (Table 15), together with a very good agreement for the melting point of the elements. Moreover, the sensitivity of differential scanning technique (DSC) during cooling was set quite high to reveal the less energetic activity associated with the order-disorder process at lower temperature.

Table 15 Melting range and enthalpy of transformation for experimental alloys

LEGA	T_{sol} - T_{liq} [°C]	ΔT [°C]	ΔH_m [J/g]	ΔT_{sat} [°C]	ΔH_{sat} [J/g]
Ag	960,9	0,0	-101,6	n.d.	n.d.
Au	1062,8	0,0	-64,46	n.d.	n.d.
B	914,2 – 921,2	7,0	-76,53	269,0 – 420,8	-14,37 – -21,49
C	903,8 – 912,3	8,5	-73,46	283,8 – 414,2	-18,21 – -10,02
D	803,2 – 892,4	89,2	-64,72	209,1 – 370,3	-13,52 – -23,60
E	859,5 – 912,7	53,2	-72,92	263,0 – 416,0	-13,41 – -19,85
F	903,6 – 911,7	8,1	-74,40	268,4 – 394,2	-12,38 – -15,73
G	792,6 – 885,2	92,6	-64,43	210,7 – 358,4	-13,15 – -21,30
H	759,8 – 881,3	121,5	-58,11	214,4 – 346,9	-10,50 – -13,95

Enthalpy measurement experiments are difficult. In order to check the accuracy of our analytical system, we compared the enthalpy of order-disorder transformation for an equimolar alloy (Au 50 at.%, Cu 50 at.%) given by literature sources with data obtained

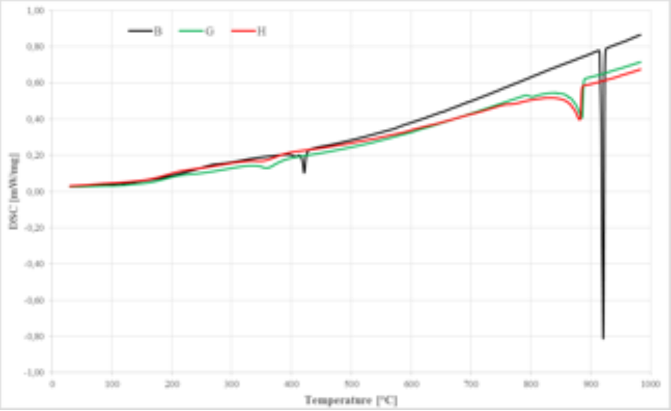

Figure 23 Differential scanning calorimetry (DSC) of complex alloys respect to AuCu matrix

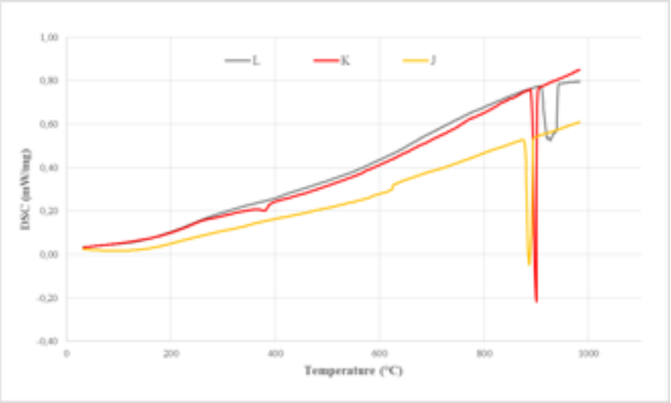

Figure 24 DSC heating run of 18K commercial alloys

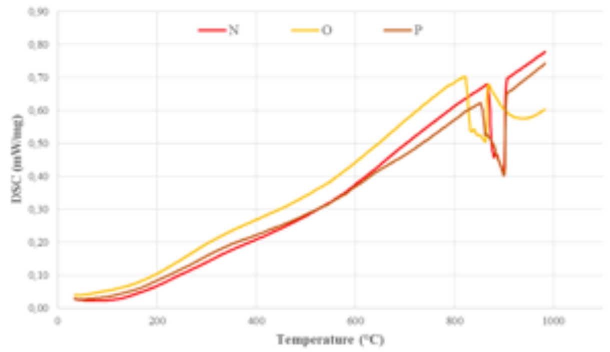

Figure 25 DSC heating run of 14K commercial alloys

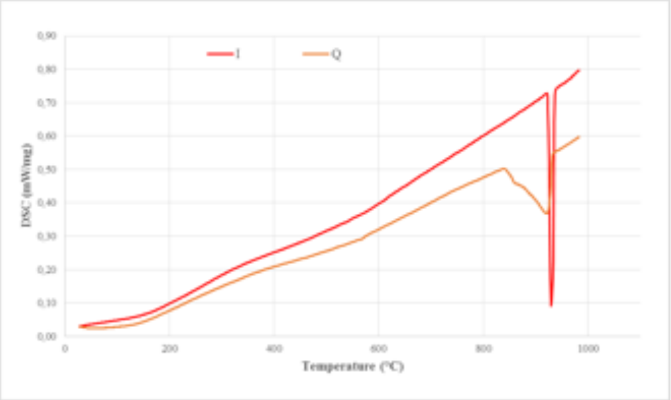

Figure 26 DSC heating run of a high fineness (21K) and a low fineness (10K) alloy

in our laboratory. A very specific publication indicates that for the homogenized alloy, the value of enthalpy for the order-disorder transformation (ΔH_{tr}) AuCu (II) – AuCu (α) can range from to 7.9 to 12.8 J/g,[15,16] depending on the technique used and measurement parameters. The value of transformation enthalpy for the same solid-state process determined in our laboratory for analogous conditions was 13.30 J/g (Figure 21). Thus, our experimentally measured enthalpy data can be considered valid.

The reference gold-copper alloy (B) presents the most restricted melting range (7°C) and, therefore, based on the initial hypothesis, it should have provided the worst filling of the series. The resulting casting, however, showed the opposite of what was expected, at least for ternary alloys. The binary alloy (B) showed a maximum filling of the grids with 67.01% while the alloy with a wider melting range (D), which is the one containing 2 at.% germanium, showed minimum form-filling compared to copper with 64.22%. However, the simple binary matrix (B) is the alloy with the highest melting enthalpy (-76.53 J/g), which means a greater energy release during solidification and, therefore, can cause a higher temperature at the investment wall of the mold cavity to improve the form-filling.

The presence of some metalloid additives can greatly widen the melting range, and they generally tend to decrease the solidus temperature (Table 15), as can be seen from phase diagrams. A clear example of this is given by germanium, which, if present at 2 at.% in a parent binary matrix (AuCu 18K), achieves a decrease of 30°C (54°F) in the liquidus temperature and 110°C (198°F) in the solidus temperature. Consequently, the melting range widens to approximately 80°C (144°F). Germanium also consistently reduces the energy required for melting, and the melting enthalpy is the lowest in the ternary series (-64.72 J/g) (Figures 22 and 23). This effect is intensified by the presence of silicon. The thermal data also confirmed the shift toward lower temperature of the order-disorder transformation in germanium alloy (D).

On the other hand, the most relevant feature encountered with commercial-like alloys is the disappearance of the order-disorder transformation in most cases (Figures 24–26), but this phenomenon is mainly due to compositions outside the stability field of the intermetallic phases (AuCu) due to copper content both too high and too low in the alloy formula (Table 16). In a coherent way with experimental alloys, the melting range widens with zinc and other low-meltingpoint additives but also diminishes the gold assay. The latter aspect is given by the relative increase of other low-melting-point elements and the increase of copper content. The low-karat alloys also have shown a higher melting enthalpy that, on one the hand, makes them harder to liquefy but, on the other hand, can help to maintain the temperature in the mold cavities.

Table 16 Melting range, enthalpy of fusion and of secondary transformations of commercial-like alloys

LEGA	T_{sol} - T_{liq} [°C]	ΔT [°C]	ΔH_m [J/g]	ΔT_{sat} [°C]	ΔH_{sat} [J/g]
I	923,4 – 929,6	6,2	-65,68	n.d.	n.d.
J	878,5 – 886,2	7,7	-66,8	n.d.	n.d.
K	891,2 – 900,1	8,9	-72,59	258,1 – 380,6	-11,67
L	909,4 – 937,4	28,0	-73,12	n.d.	n.d.
N	869,0 – 899,7	30,7	-86,49	n.d.	n.d.
O	823,3 – 862,2	38,9	-72,70	n.d.	n.d.
P	853,8 – 899,8	46,0	-85,88	n.d.	n.d.
Q	841,2 – 922,8	81,6	-99,88	n.d.	n.d.

Specific Heat

The specific heat of metals in the solid state is typically lower compared to the molten state (Table 17). This presumably happens because the molten state at a high temperature requires a significantly higher quantity of energy to further increase the temperature of an already hot material. Theoretically, in casting processes, the determination of the casting heat should be done during the cooling phase for the molten metal and during the heating phase for the mold material, because the mold is the receiver of all the thermal energy that the metal releases during the solidification phase.[17] However, because of vaporization of some alloy components and the small sample mass (85 mg), it was difficult to make accurate measurements during the cooling steps of the analysis. Because the same investment mold was used for all casting trials, specific heat measurements on this material were not done.

Table 17 Specific heat of the main metallic elements[15]

ELEMENT	Cp_{RT} [J/gK]	Cp_{liq} [J/gK]
Gold	0,13	0,15
Copper	0,39	0,49
Silver	0,23	0,28
Zinc	0,39	0,48
Tin	0,21	0,24
Silicon	0,71	0,91
Nickel	0,44	0,73
Palladium	0,24	-
Gallium	0,37	-
Cobalt	0,42	0,69
Iridium	0,13	0,18
Rhodium	0,24	0,39
Platinum	0,13	0,18
Niobium	0,27	0,35
Titanium	0,54	0,79
Iron	0,46	0,82
Aluminum	0,92	1,18
Beryllium	1,82	3,27
Manganese	0,48	0,84

Thus, the measurement of the specific heat was operated with a quite fast heating rate (20°C/min–36°F/min), from close to room temperature up to 1200°C (2192°F) in order to have a quite

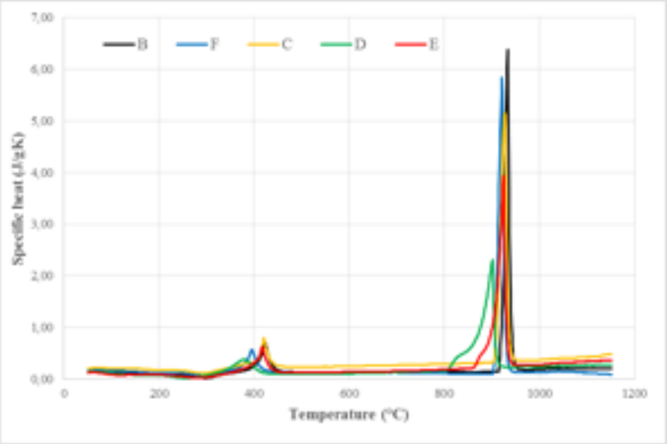

Figure 27 Specific heat as a function of the temperature for the 18K experimental ternary alloys

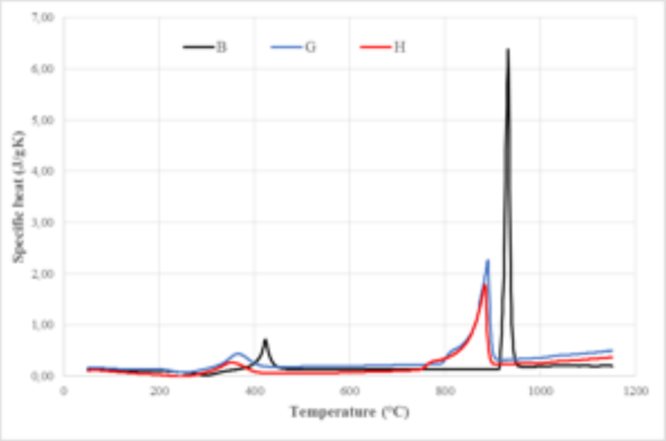

Figure 28 Specific heat as a function of the temperature for the 18K complex experimental alloys

linear segment for better extrapolation of data after melting. During phase transitions, the specific heat values are neglected because in this range those values have no physical meaning. The meaningful value for the specific heat is the one calculated slightly above the liquidus temperature because it is the point with the smallest composition alterations.

The magnitude of specific heat is related not only to the ability of materials to increase their temperature but also to the potential capacity to store thermal energy. In a first approximation, it is possible to say that higher specific heat values in molten metals translate into a longer life of the liquid state. The experimental alloys with the highest specific heat in the liquid state were, in most cases, those having metalloid elements (Figures 27 and 28) because they have a more refractory behavior (Table 18).

Table 18 Specific heat of the 18K experimental alloys

ALLOY	Cp_{RT} [J/gK]	Cp_{liq} [J/gK]
A	0,132	0,293
B	0,130	0,192
C	0,200	0,367
D	0,145	0,241
E	0,119	0,277
F	0,180	0,143
G	0,163	0,319
H	0,109	0,238

CONCLUSIONS

In the past[18] it was assumed that the contribution of a component metal to the density of an alloy was linearly related to the density and concentration of this metal in the alloy, thus making it possible to calculate the value for the density of the alloy as a whole. Deviation from this behavior occurs in the alloys formed by the metals of the copper group, and this is significant in the study of gold alloys. Although the pure elements gold, silver and copper and their binary and ternary alloys crystallize mainly in the face-centered cubic form, the densities of these alloys do not display a linear correlation with the chemical composition (at.%). This is due mainly to the effects of ordering and disordering in the alloys as is described in this paper. Therefore, it is no longer necessary to generate models and formulas in order to calculate these properties since we demonstrate that it is possible to experimentally obtain these parameters for each alloy.

The form-filling of patterns and, thus, the castability of an alloy are strongly influenced by the chemical composition because the variety of elements present in its composition acts directly on its thermodynamic and volumetric properties. The metalloid or low-melting elements can increase the castability of an alloy only if present in certain concentrations and combinations. For example, a red alloy (18K) can show an improvement in castability if it only contains 1 wt.% of silver or if the combination of zinc and germanium is about 1wt.%. The eventual addition of silicon to this last composition can further increase the degree of form-filling, but there is the risk of having more shrinkage defects due to the fact that the alloy presents a higher density change in the melting range.

The addition of other elements into a gold matrix is a practical inevitability because they confer to the alloy the right mechanical resistance, hardness and color. However, these additions aid castability only if the incorporated elements reach certain concentrations and have an effect on the fusion temperature, surface tension in the molten state, and density change across the melting range. The presence of deoxidant additives (Si, Ge) also has a protective role at the molten state because they continuously eliminate the metal oxides, thus avoiding the formation of hard spots and brittleness.

The castability of a precious alloy also seems to depend on the density change across the melting range, along with other physical properties such as the characteristic melting temperatures and the surface tension and viscosity in the molten state, which are known aspects from the literature.[7,19] This phenomenon appears to be valid for most of the alloys analyzed, with few exceptions.

In particular, a higher density change during solidification seems to correspond to a higher filling capacity. Pure gold and silver show a large density change ($\Delta d_{sol\text{-}liq(Au)}$ = 1.015 g/cm^3, $\Delta d_{sol\text{-}liq(Ag)}$ = 0.533 g/cm^3) while going from the liquid state ($T_{m(Au)}$ = 1064°C, $T_{m(Ag)}$ = 961°C) to the solid state, and this produces high form-filling (72.56% and 82.48%, respectively). Copper, on the other hand, even though it has a fusion temperature very similar to that of gold (T_{liq} = 1084°C), shows a lower density change ($\Delta d_{sol\text{-}liq(Cu)}$ = 0.384 g/cm^3) and exhibits lower formfilling (59.64%).

The filling capacity of these metals (Au, Ag, Cu) is also influenced by their surface tensions in the liquid state, which is a property proportional to the internal cohesive forces of the material. A higher surface tension corresponds to a very strong bond between the atoms in the molten state and, consequently, the liquid tends to expand its surface less. Consequently, this fact implies a lower capacity to fill the patterns. Silver's surface tension (σ_{liq} = 910 mN/m) is the lowest and thus its filling is the highest,19,20 while the surface tension of gold is intermediate (σ_{liq} = 1138 mN/m) and its filling capacity is also intermediate. Copper is the element possessing the highest surface tension (σ_{liq} = 1355 mN/m) among these three metals that constitute the basic matrix in jewelry and, as a consequence, its form-filling is lowest.

Yet, the addition of elements (2 at.% Zn) that further lower the surface tension[20] did not give the expected increase in form-filling and, thus, castability, demonstrating that the surface tension of the alloy cannot be the only determining factor in predicting this metallurgical behavior. Furthermore, a low surface tension typical of low-karat alloys (14K) or of higher karats (18K) with Zn does not necessarily correspond to an elevated density change across the melting range and, consequently, to a high filling capacity, as shown for some alloys in the paper (C, O). It must be highlighted once again that density change across the melting range can play a very important role in the castability of an alloy.

Castability also depends on the difference between the mold temperature (650°C) and the characteristic temperatures of the alloy, because this determines the cooling rate of the melt. Alloys with melting temperatures (T_{sol}, T_{liq}) close to the flask temperature should provide a higher filling but, based on what was observed in some experimental alloys (C, D, E), this is not always true because the filling was lower with respect to the gold-copper matrix (B). Only when additive elements exceed a given atomic percentage (G, H) does density change across the melting range and the decrease of the fusion temperatures reach a point where they surpass the castability of the matrix.

Parallel to the increase of castability, there is also an increase of the uniformity of filling along the casting tree. This increase in uniformity is even higher in the castings aided by pressure (K), except in the case of flasks with no openings. A higher uniformity is reached both with metals that show low melting points and with alloys that show an ample melting range. The perforation opening degree of the flasks seems to influence filling only in the cases when casting is aided with vacuum pressure and in the case of small openings (Ø < 4 mm). In the case of larger openings or castings executed only with gravity, the opening degree does not influence the filling of the patterns in a considerable way. The vacuum pressure technique amplifies the filling of the patterns by about 30–50% over the values obtained by gravity under laboratory conditions.

The additive elements that increase such uniformity in a consistent way are germanium and silver. In commercial alloys the effect of additives was clearly demonstrated by comparing the results of a dilatometry tests of an alloy containing gallium (P) and its equivalent without gallium (P*). The presence of this element diminished the density change across the melting range by about 20%. This happens because metalloid elements supply a denser liquid phase and a more voluminous liquid phase.

In an analogous way, the effect of a typical grain refiner on filling of the patterns was studied by performing the casting of one alloy (K) and its counterpart without the grain refiner using the same casting parameters. The effect of the grain refiner seems to increase the filling (+0.60%), but this improvement gives a value that resides within the uncertainty of the measurement and consequently it is not decisive.

An interesting result was the confirmation of the correlation that relates the alloy composition directly to the average coefficient of linear thermal expansion (CTE_a) of the alloy. In practice, the CTE_a of the alloy is a weighted average of the coefficients of linear thermal expansion of the pure elements accordingly to their atomic fractions (Equation 2), giving a measurement error that is less than 10% between the calculated and experimental value. This correlation allows one to quickly estimate the CTE_a of a precious metal alloy, knowing only the chemical composition.

Metallurgical operations at elevated temperatures such as those that involve solidification and/or mechanical deformation, can be critically influenced by the thermal stresses and strains that result from expansion and contraction of the material as a function of temperature. With the increasing use of computer-based process models for these operations, there arises a greater need for quantitative data on the thermal expansion coefficient of the relevant alloy at the temperatures involved.[3] In the future, dilatometry, form-filling and thermal analysis tests of silver alloys will be performed in order to learn whether the same additive elements have analogous effects in that alloy system.

ACKNOWLEDGEMENTS

Many thanks for the support of Doreen Rapp, Appliations Laboratory of Netzsch Group, for her kindness and long-term availability.

REFERENCES

1. D. Schneller, "The Cave of Treasures: Lost Wax Castings from 3500 B.C.," *The Santa Fe Symposium on Jewelry Manufacturing Technology 1987*, ed. D. Schneller (Boulder, CO: Met-Chem Research, 1988): 1–28.
2. "Defects analysis and classification of the most common problems in the production processes of gold alloys"; http://www.progold.com/GB/Files/ Publications/defects%20 handbook_eng.pdf.
3. J.D. James et al., "A review of measurement techniques for the thermal expansion coefficient of metals and alloys at elevated temperatures," *Measurement Science and Technology* 12, no. 3 (March 2001): R1–R15.
4. www.wikipedia.org.
5. Dieter Ott and Christoph J. Raub, "Investment Casting of Gold Jewellery: Factors influencing the filling of moulds," *Gold Bulletin* 19, no. 2 (1986).
6. Dieter Ott and Christoph J. Raub, "Investment Casting of Gold Jewellery: Factors influencing the filling of moulds," Gold Bulletin 18, no. 2 (1985): 58–68.
7. J.A. Tesk et al., "The mesh monitor for casting characterization," Noble Metals Fabrications & Technology Seminar, International Precious Metals Institute, ed. Dr. Leah Gal-Or: 35.
8. V.G. Rivlin et al., "The structure of gold alloys in the liquid state: novel quench products from some eutectic systems," *Gold Bulletin* 9, no. 3 (September 1976): 84–87.
9. David R. Lide, *Handbook of Chemistry and Physics*, 87th ed. (CRC Press, 2006– 2007).
10. "Properties and Selection: Nonferrous Alloys and Special-Purpose Materials," *ASM Handbook 2*, 10th ed. (October 1, 1990).
11. www.engineeringtoolbox.com.
12. Dr. G.M. Ingo et al., "Thermal Stability and Chemical Physical Features of Gypsum-Bonded Investment with Regard to Burnout Cycle," The Santa Fe Symposium on Jewelry *Manufacturing Technology 2005*, ed. E. Bell (Albuquerque: Met-Chem Research, 2005): 255.
13. P. Sbornicchia, "Development and characterization of refractory moulds for lost investment casting," Ph.D. thesis, University of Tor Vergata, Rome, Italy (2001–2003).
14. A.F. Crawley, "Densities of Liquid Metals and Alloys," *International Metallurgical Reviews* 19, no. 1 (1974).
15. Y. Feutelaisa et al., "New enthalpies determination and in situ X-ray diffraction observations of order/disorder transitions in Au0.5Cu0.5," *Acta Materialia* 47, no. 8 (22 June 1999): 2539–2551.
16. Djamel Hamana et al., "The apparition of a new reaction at lower temperature in equiatomic CuAu alloy," *Phase Transition* 82, no. 10 (October 2009): 755–766.
17. Juan J. Valencia and Peter N. Quested, "Thermophysical Properties," ASM *Handbook: Casting* 15 (ASM International, 2008): 468–481.
18. J.C. Kraut and W.B. Stern, "The density of gold-

silver-copper alloy and its calculation from the chemical composition," *Gold Bulletin* 33, no. 2 (2000).
19. Robert E. Reed-Hill and Reza Abbaschian, *Physical Metallurgy Principles*, 3rd ed. (Cengage Learning, 1991).
20. E. Ricci and R. Novakovic, "Wetting and Surface Tension Measurements on Gold Alloys," *Gold Bulletin* 34, no. 2 (2001): 41.
21. W.S. Rapson and T. Groenewald, *Gold usage* (Academic Press, 1978).
22. D. Pinton, *Tecnologia Orafa. Processi Produttivi, Mezzi Strumenti* (Gold Editions).
23. Dieter Ott, *Handbook on Casting and Other Defects in Gold Jewellery Manufacture* (London: World Gold Council, 1997).